Flame-Retarding Mechanism of Organically Modified Montmorillonite and Phosphorous-Nitrogen Flame Retardants for the Preparation of a Halogen-Free, Flame-Retarding Thermoplastic Poly(ester ether) Elastomer

Yuhua Zhong, Wei Wu, Xingqing Lin, Maolin Li

Sino-German Joint Research Centre of Advanced Materials, School of Materias Science and Engineering, East China University of Science and Technology, Shanghai, 200237, People's Republic of China
Correspondence to: W. Wu (E-mail: wuwei@ecust.edu.cn)

In this study, thermoplastic poly(ester ether) elastomer (TPEE) nanocomposites with phosphorus–nitrogen (P–N) flame retardants and montmorillonite (MMT) were prepared by melt blending. The fire resistance of the nanocomposites was analyzed by limiting oxygen index (LOI) and vertical burning (UL 94) tests. The results show that the addition of the P–N flame retardants increased the LOI of the material from 17.3 to 27%. However, TPEE containing P–N flame retardants only obtained a UL 94 V-2 ranking; this resulted in a flame dripping phenomenon. On the other hand, TPEE containing the P–N flame retardant and organically modified montmorillonite (o-MMT) achieved better thermal stability and good flame retardancy; this was ascribed to its partially intercalated structure. The synergistic effect and synergism were investigated by Fourier transform infrared spectroscopy and thermogravimetry. The introduction of o-MMT decreased the inhibition action of the P–N flame retardant and increased the amount of residues. The catalytic decomposition effect of MMT and the barrier effect of the layer silicates are discussed in this article. The residues after heating in the muffle furnace were analyzed by scanning electron microscopy, energy-dispersive X-ray spectroscopy and laser Raman spectroscopy. It was shown that the intercalated layer silicate structure facilitated the crosslinking interaction and promoted the formation of additional carbonaceous char residues in the formation of the compact, dense, folded-structure surface char. The combination of the P–N flame retardant and o-MMT in TPEE resulted in a better thermal stability and fire resistance because of the synergistic effect of the mixture. © 2014 Wiley Periodicals, Inc. J. Appl. Polym. Sci. **2014**, *131*, 41094.

INTRODUCTION

Thermoplastic poly(ester ether) elastomers (TPEEs) consist of both hard and soft segments, in which the hard segments are crystalline poly(butylene terephthalate)s and the soft segments are amorphous polyethers.[1] TPEEs have already proven their performance for a wide variety of applications in automotive and various other industrial and consumer products. However, TPEEs are easily ignited and rapidly burned. Therefore, it is urgent that we enhance their fire resistance to meet the requirements of fire safety. There have been few reports on their flame-retardation characteristics. Flame retardants are widely used for thermoplastic polyesters as halogenated additives, yet they are most often brominated as polymeric materials, and their synergism originates in antimony.[2] Recently, because of calls for environmental protection, the demand for flame-retardant performances and the disposal of waste materials is

on the rise.[3] Consequently, the preparation and development of halogen-free materials has become extremely urgent.

Generally, halogen-containing fire retardants are considered to be effective. However, there has been increasing interest in the use of halogen-free flame retardant substances. Many more efforts have been made to use phosphorus-based compounds for flame retardants.[4–7] Researchers have reported that phosphorus–nitrogen (P–N) flame retardants must cooperate with other synergistic agents to prepare excellent flame-retarding thermoplastic esters.[8,9]

The application of nanoscale fillers in the improvement of the thermal and combustion properties of polymer nanocomposites has been a hot spot in the field of flame-retardant research.[6,10–12] Over the past 20 years, polymer layered-silicate nanocomposites (PLSNs) have received considerable attention in fundamental

Table I. Compositions of the Formulations

	Material	TPEE (wt %)	P–N (wt %)	Na-MMT (wt %)	o-MMT (wt %)
1	TPEE	100	-	-	-
2	TPEE/P–N	90	10	-	-
3	TPEE/P–N/Na-MMT	88	10	2	-
4	TPEE/P–N/o-MMT	88	10	-	2

research and industrial applications. Compared to conventional filled polymers, PLSNs have a lot of unique properties in the presence of a small amount of silicate, such as enhanced mechanical properties, increased heat-distortion temperatures, improved thermal stability, decreased gas/vapor permeability and reduced flammability.[13,14] The use of P–N flame-retarding montmorillonite (MMT) as a flame-retardant synergist for flame-resistant thermoplastics such as PP, PA6, and PA66 has been reported.[15–21]

In this research, we developed novel formulations for flame-retarding TPEEs and gave insight into the synergism between the P–N flame retardant and organically modified montmorillonite (o-MMT). Our focus was on the chemical reaction of the ternary component and char formation during the heating process.

EXPERIMENTAL

Materials
TPEE (H3030, weight-average molecular weight $\approx$ 30,000) was purchased from Sunplas Co. (China). Aluminum diethyl phosphinate (AlPi; OP1230) was purchased from Clariant (Germany). Melapur 200 (MPP) was supplied by Ciba/BASF. The P–N flame retardant consisted of Aluminum diethylphoshinate (AiPi) and MPP (2:1 w/w). Sodium montmorillonite (Na-MMT), with a cationic exchange capacity of 90 mequiv/100 g, was supplied by Nanocor. The o-MMT was a commercial organophilic MMT (Nanomer 1.44P, Nanocor) that had been modified with dimethyl dialkyl ammonium halide. TPEE was dried in an oven at 100°C for 5 h before compounding; Na-MMT and o-MMT were dried in an oven at 105°C for 5 h before being added to the mixture. Other additives were used as received. All of the investigated formulations are given in Table I.

Sample Preparation
The TPEE pellets were melt-mixed with the additives in a twin-roll mill at a temperature of 200–210°C for 10 min. After mixing, all of the samples were hot-pressed under 12 MPa for 5 min at about 210°C to obtain a sheet of suitable thickness and size for analysis.

Measurements
Limiting Oxygen Index (LOI). LOI was measured according to ASTM D 2863. The apparatus used was an HC-2 oxygen index meter (Jiangning Analysis Instrument Co., China). The specimens used for the test had the following dimensions: $130 \times 6 \times 3$ mm^3.

UL 94 Testing. The vertical test was performed according to ASTM D 3801. The apparatus used was a CFZ-2 type instrument (Jiangning Analysis Instrument Co., China). The dimensions of the sample were $130 \times 13 \times 1.6$ mm^3.

Morphological Characterization. X-ray diffraction (XRD) was performed on a sheet 1 mm thick with a Scinatag diffractometer in a θ–θ geometry with Cu Kα radiation ($\lambda = 1.54$ nm) operated at 45 kV and 40 mA at room temperature. The scanning diffractograms were scanned from 1.5 to 10° in the 2θ range with step size at 0.02°, and the scanning rate was 3°/min.

The morphological structure of the composites was investigated with a Hitachi H-600 transmission electron microscope (Japan) with an acceleration voltage of 100 kV.

Thermal Analysis. Thermogravimetric analysis (TGA) was measured with a Netzsch STA 409 PC/PG thermogravimetry (TG) analyzer. Experiments were conducted with 8–10 mg samples heated in flowing nitrogen (20 mL/min) at a heating rate of 10°C/min. The calculated TG and derivative thermogravimetry (DTG) curves were obtained according the following equation:[22]

$$M_{cal}(T) = \chi_i W_i \tag{1}$$

where M_{cal} is mass loss in the real time temperature through the equation calculation, T is real time temperature, χ_i is the content of compound i and W_i is the TG curve of compound i.

Fourier Transform Infrared (FTIR) Spectroscopy. FTIR spectra were measured with a Nicolet 5700 spectrophotometer equipped with a ventilated oven and a heating device in the range 400–4000 cm^{-1} with a resolution of 4 cm^{-1}. We made the films by melting sample powder on a KBr disc and heating it from room temperature to 400°C at a heating rate of 10°C/min under an air atmosphere.

Residue Analysis. The composites were burned by a furnace-burning test at 800°C for 10 min in a muffle furnace to introduce thermooxidation char during combustion. The morphology and elemental content of the residues were scanned with scanning electron microscopy (SEM)–energy-dispersive X-ray spectroscopy (EDX; S-4800, Hitachi, Japan).

Laser Raman spectroscopy measurements were carried out at room temperature with an ASPEX-1043 laser Raman spectrometer (SPEX Co.) with excitation provided in backscattering geometry with a 514.5 nm argon laser line.

RESULTS AND DISCUSSION

Characterization of the Composites
Figure 1 shows the XRD patterns of Na-MMT, o-MMT, TPEE/P–N/Na-MMT, and TPEE/P–N/o-MMT. The interlayer distance (d), calculated with the Bragg's law equation, is presented in Table II. As is shown in Figure 1, a diffraction peak around $2\theta = 6.98°$ was displayed by Na-MMT. A diffraction peak at $2\theta = 4.13°$ was displayed in the sample of o-MMT. The basal spacing of MMT increased with organic modification from 1.26 to 2.14 nm. This indicated that layered silicates were intercalated by organic quaternary ammonium salts.

XRD of TPEE/P–N/Na-MMT did not show any peaks with the same d-spacing as the Na-MMT. This may have been an indication that Na-MMT was not nano-dispersed in the materials for the immiscible dispersion and low contents. The diffraction
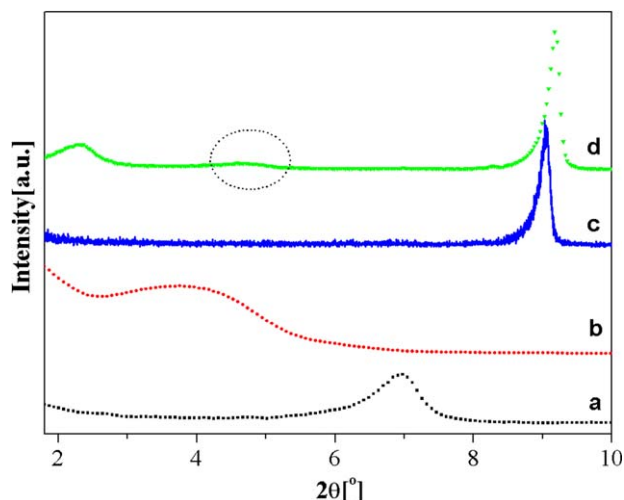
Figure 1. XRD patterns of (a) Na-MMT, (b) 1.44P, (c) TPEE/P–N/Na-MMT, and (d) TPEE/P–N/o-MMT. [Color figure can be viewed in the online issue, which is available at wileyonlinelibrary.com.]

peak around $2\theta = 9.04°$ and corresponding to an 0.98 nm interlayer distance was attributed to the introduction of flame-retardant additives.

There were different results when o-MMT was used in the composites: the diffraction peaks of TPEE/P–N/o-MMT were observed at a lower angle than that of o-MMT; this indicated an increase in the basal spacing. This result indicated that the TPEE molecular chains intercalated and expanded in the galleries of o-MMT; that is, a multilayer structure consisting of alternating TPEE molecular chains stacked with the silicate layers was created in the composite. The decreased intensity of the based reflection of TPEE/P–N/o-MMT may have resulted from the delamination of the silicate layer.[2,23] The correspondence between the $2\theta = 4.58°$ peak and the 1.93 nm interlayer distance indicated that tactoids were distributed in the materials. A diffraction of the P–N flame-retardant additive peak at $2\theta = 9.2°$ was also observed.

It was difficult to draw definitive conclusions about the defined structure from XRD. The XRD data alone gave a partial picture of the clay distribution.[24,25] The XRD results were complemented by structural analysis with transmission electron microscopy (TEM). The morphology of TPEE/P–N/o-MMT was further confirmed by TEM (Figure 2). As demonstrated in Figure 2, the individual clay layers were observed to be well-dispersed in the TPEE matrix (showing exfoliation). However, tactoids in the matrix were also present (dark zone). The image shows an intercalated morphology in which the distance

Table II. XRD Results and Calculated Interlamellar Distances for the Clays and Composites

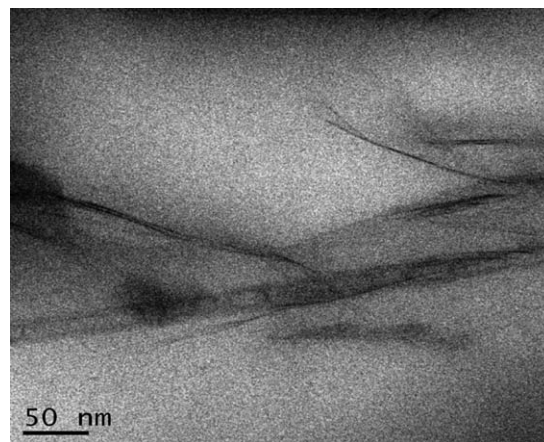|	Na-MMT	o-MMT	TPEE/P–N/Na-MMT	TPEE/P–N/o-MMT		
				1	2	3
2θ (°)	6.98	4.13	9.04	2.30	4.58	9.19
d (Å)	12.65	21.37	9.78	38.13	19.27	9.61

Figure 2. TEM micrograph of TPEE/P–N/o-MMT.

between adjacent layers was about 2 nm. The TEM images of TPEE/P–N/o-MMT revealed that the clay layers consisted of multilayered stacks, and some intercalated silicate layers were observed. In addition, the clay mineral layers were delaminated in the TPEE matrix in the TPEE/P–N/o-MMT composites.

Thermal Stability

Thermal degradation behaviors of the flame-retardant TPEE composites were investigated by TG, and the results and the curves are presented in Figures 3 and 4 and summarized in Table III, respectively.

The addition of the P–N flame-retardant additives, Na-MMT, o-MMT and their mixture into TPEE increased the initial decomposition temperature, the maximum decomposition temperature, and the weight of remaining residue at high temperature. The results also show that the addition of the flame-retardant additives reduced the mass loss rate of the materials. Above all, the P–N flame-retardant additives and nanoclay promoted the thermal stability of TPEE.

The initial decomposition temperatures of formulation 3 (373.3°C) and formulation 4 (371.4°C) were lower than the
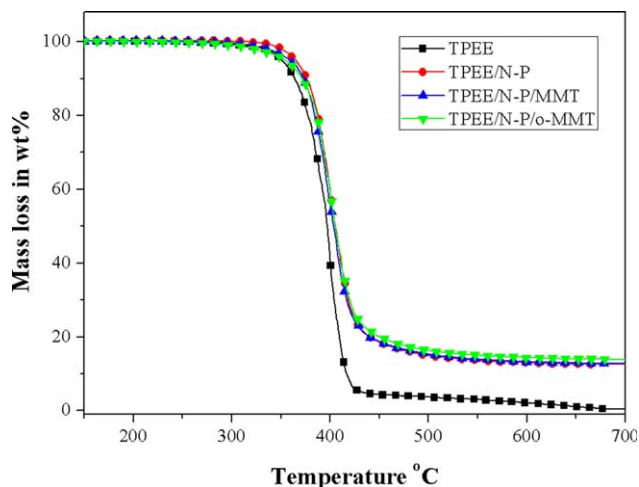

Figure 3. Mass loss curves of all of the samples recorded under an N_2 atmosphere (heating rate = 10°C/min). [Color figure can be viewed in the online issue, which is available at wileyonlinelibrary.com.]
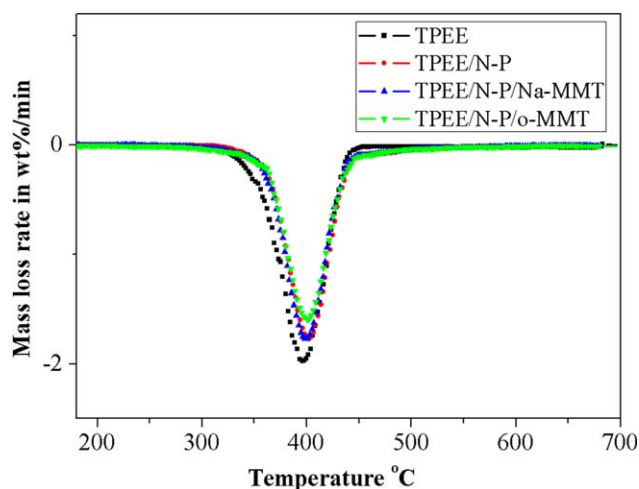
Figure 4. Mass loss rate curves of all of the samples recorded under an N_2 atmosphere (heating rate = 10°C/min). [Color figure can be viewed in the online issue, which is available at wileyonlinelibrary.com.]

Figure 5. Mass loss curve of the P–N mixture flame retardant and o-MMT at a mass ratio of 10:2 (heating rate = 10°C/min, N_2 flow). [Color figure can be viewed in the online issue, which is available at wileyonlinelibrary. com.]

initial decomposition temperature of formulation 2 (376.5°C). The lower initial decomposition temperatures might have resulted from the catalytic effect of the nanoclays on the fragmentation of the macromolecular chain. The presence of photonic catalytic sites could have catalyzed char crosslinking interactions to form a charred residue, which combined and intercalated with the silicate layers to provide a sort of char–layered-silicate nanocomposite.[4,23–26] The residue at the high temperature increased for Na-MMT and was replaced by the same amount of o-MMT. The research results show that no trace of char would be observed regardless of the amount of incorporated Na-MMT. Another study suggested, however, that the dispersion state of the clay particles in the polymer matrix may have had a considerable influence on the flammability.[27] Formulation 4 led to the best thermal stability of the materials for the highest char residue amount and the lowest mass loss rate. The results might have come from a synergistic effect between the o-MMT and P–N flame-retardant additives.

To understand the synergistic effect between the P–N flame retardant and o-MMT during the decomposition process, the TG curves of the P–N flame retardant, o-MMT, and P–N/o-MMT (mass ratio = 5:1) in nitrogen are presented in Figure 5, and the results are summarized in Table IV.

The initial decomposition temperature of P–N/o-MMT shifted to 342.7°C; this was lower than the calculated one (392.5°C), and the temperature of the maximum loss rate decreased to 464.6°C. These phenomena demonstrated that o-MMT promoted the decomposition of the P–N flame retardant for its catalytic effect. However, the experimental TG curve was above the calculated one after 550°C, and more remaining residues in the condensed phase were obtained compared to the calculated one at 700°C. The results demonstrate that o-MMT reduced the gas-phase flame-retarding effect of the P–N flame retardant and strengthened the action of the condensed phase. All of the results showed that a strong interaction between the o-MMT and P–N flame-retardant system occurred during the thermal degradation process.

Combustion Behavior

The results of the LOI and the UL 94 tests are given in Table V. Neat TPEE was an inflammable material, with a LOI of 17.3%, and it failed the UL 94 test (no rating). Therefore, it was important to improve its flame resistance. The addition of 10 wt % P–N flame retardant increased its LOI value to 31% and

Table III. Decomposition Temperatures of All of the Formulations at a Heating Rate of 10°C/min in a Nitrogen Atmosphere

	Material	T_{onset} (°C)	T_{max} (°C)	Residue (wt %)
1	TPEE	363.9	395.5	0.39
2	TPEE/P-N	376.5	401.9	12.54
3	TPEE/P-N/Na-MMT	373.3	397.8	12.76
4	TPEE/P-N/o-MMT	371.4	400.7	13.89

T_{onset}, temperature of 10 wt % mass loss; T_{max}, temperature of the maxium mass loss rate in DTG curves
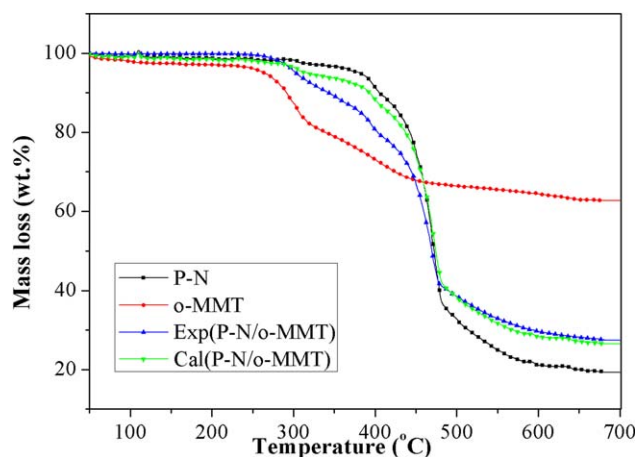
Table IV. Data Recorded in the Mass Loss Curve of the P–N Mixture Flame Retardant and o-MMT at a Mass Ratio of 10:2 (Heating Rate = 10°C/min, N_2 Flow)

	Material	T_{onset} (°C)	T_{max} (°C)	Residue (wt %)
1	P-N flame retardant system	405.2	472.8	19.3
2	o-MMT	291.3	404.9	62.6
3	Experimental P-N/o-MMT	342.7	464.6	27.4
4	Calculated P-N/o-MMT	392.5	475.1	26.5

T_{onset}, temperature of 10 wt % mass loss; T_{max}, temperature of the maxium mass loss rate in DTG curves

Table V. LOI and UL 94 Test Results of the Investigated Formulations

	Material	LOI (%)	Ranking	Dripping	t_1/t_2 (s)[a]
1	TPEE	17.3 ± 0.5	No rating	-	-
2	TPEE/P–N	31 ± 0.5	V-2	No/yes[b]	1.4/2.5
3	TPEE/P–N/Na-MMT	29.5 ± 0.5	V-2	-	-
4	TPEE/P–N/o-MMT	29 ± 0.5	V-0	No/no	4/0

[a] t_1 and t_2, average combustion times after the first and second applications of the flame, respectively.
[b] No and yes correspond to the first and second flame applications, respectively.

improved its UL 94 rating to V-2. However, the P–N flame retardant failed to prevent flame dripping, and thus, it got only a V-2 classification. The addition of Na-MMT to TPEE/10AlPi allowed the LOI value to decrease from 31 to 29.5%. The addition of the Na-MMT obviously decreased the LOI value in comparison to that of formulation 2. In our study, the samples containing MMT had a higher char-forming speed than those composites containing no MMT in the LOI and UL 94 tests. The catalytic effect of MMT may have been caused the fast char formation, which could be explained the decrease in LOI. The combination of the P–N flame retardant and Na-MMT resulted in a V-2 ranking. The Na-MMT dispersed in the matrix was aggregated silicate layers, and this strongly suggested an immiscible dispersion. The result corresponded to the results of XRD. Na-MMT was replaced by the same amount of o-MMT in formulation 4, and the LOI value changed from 29.5 to 29%; this improved the UL 94 rating to V-0. The decrease in the LOI value resulted in the organic modification of MMT. The correlation between the LOI and UL 94 rating is not self-evident. The result from each test is the outcome of two different mechanisms: flame inhibition and charring.[27] The significant differences between Na-MMT and o-MMT were highlighted in the UL
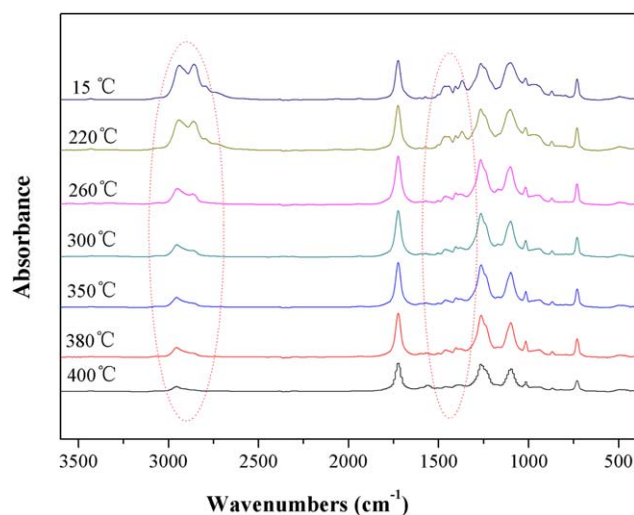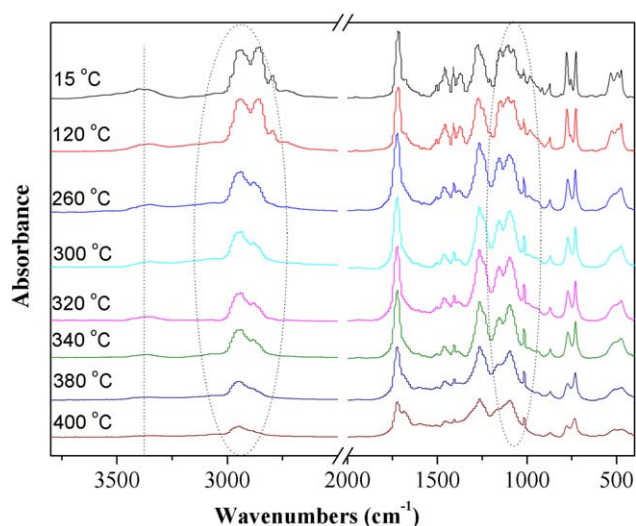

Figure 7. FTIR spectra of the solid phase in TPEE/P–N at different temperatures. [Color figure can be viewed in the online issue, which is available at wileyonlinelibrary.com.]

94 test. The results also indicate the significant differences in the microstructure in the polymer matrix, which were provided by XRD and TEM. The melt viscosity of the TPEE/P–N/o-MMT system increased dramatically for the intercalated structure; this was caused by the addition of o-MMT, and this behavior was beneficial for dripping suppression.[13,18,21,24] The catalytic effect of o-MMT decreased the LOI value but improved the UL 94 rating.

FTIR Analysis

Figures 6–9 present the alternation of the characteristic bands in the FTIR spectra obtained from the thermooxidative decomposition of the neat TPEE, TPEE/P–N, TPEE/P–N/Na-MMT, and TPEE/P–N/o-MMT composites, respectively, in the condensed phase at a heating rate of 10°C/min.

Figure 6. FTIR spectra of the solid phase in TPEE at different temperatures. [Color figure can be viewed in the online issue, which is available at wileyonlinelibrary.com.]
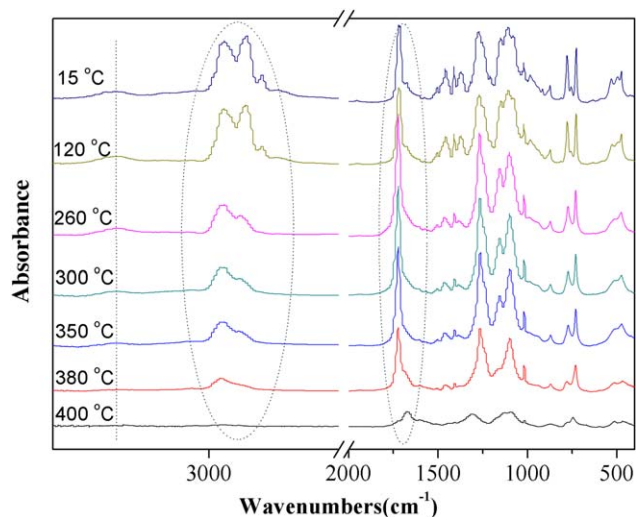

Figure 8. FTIR spectra of the solid phase in TPEE/P–N/Na-MMT at different temperatures. [Color figure can be viewed in the online issue, which is available at wileyonlinelibrary.com.]

Figure 9. FTIR spectra of the solid phase in TPEE/P–N/o-MMT at different temperatures. [Color figure can be viewed in the online issue, which is available at wileyonlinelibrary.com.]

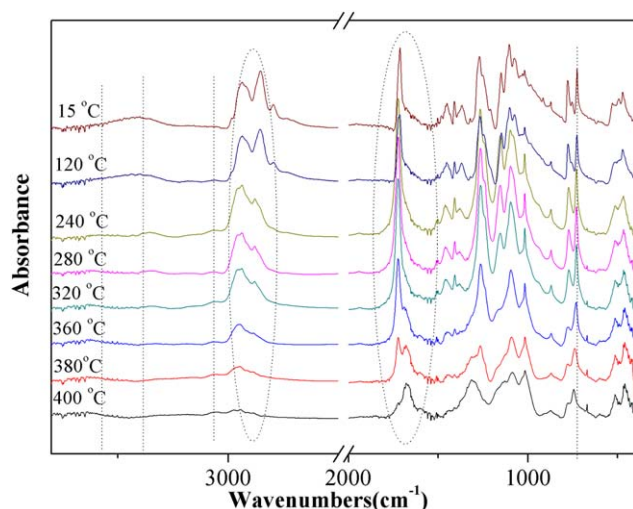The characteristic bands of TPEE were located at 2956 and 2861 cm^{-1} (—CH_2, stretching vibrations), 1715 cm^{-1} (—C═O, stretching vibrations), 1458 cm^{-1} (—CH_2, scission vibrations), 1411 cm^{-1} (aromatic ring), 1270 cm^{-1} (—CO—O esters), 1100 cm^{-1} (—CH_2—O—CH_2— ether), and 727 cm^{-1} (—CH, bending vibrations of the aromatic ring). The decomposition of the neat TPEE in the solid residue at different temperatures was measured by temperature-dependent FTIR spectroscopy (Figure 6). The intensities of the bands at 2956 and 2861 cm^{-1} (—CH_2) decreased rapidly with increasing heating temperature. The gradually disappearing peak resulted from the chain scission of the α-methylene group in the soft segments; this was demonstrated in our previous work.

Compared with the curve of the pure TPEE, the typical absorption bands of the P–N flame retardant were at 3413 cm^{-1} (—OH, MPP); 1150, 1079, and 780 cm^{-1} (—P—O); 1013 cm^{-1} (—PO_4^{3-}); 531 cm^{-1} (O—P—O, MPP); and 474 cm^{-1} (O═P—O, AlPi).[28–32] As shown in Figure 7, the chemical alteration of the TPEE flame-retarded P–N additives was investigated by FTIR spectroscopy. The flame-retarded TPEE decomposition first occurred at the long-chain soft segment because of the active α-methylene group of the ether linkage. There was a shoulder peak at 1679 cm^{-1} for carbonyl groups in the hard segments (C═O) observed for the presence of the carboxyl group (COOH). As the temperature increased to 400°C, the shifting behavior of this characteristic peak resulted from the strong interaction between carboxyl groups and aluminum ion (Al^{3+}). The typical absorption bands of the carboxy C═O located at 1683 cm^{-1} was caused by the migration of the electron. The interaction between aluminum ion (Al^{3+}) and the carboxyl group formed intermediate products; this enhanced the thermal stability of the composites. The absence of the peak at 3400–3800 cm^{-1} at 400°C revealed that there was no P—O—H unit in the residue and that the diethylphosphinic acid was released and acted as a flame inhibitor in the gas phase. The characteristic bands at 1170 and 715 cm^{-1} assigned to the aluminum phosphates and typical bands at 737 and 1411 cm^{-1} for the aromatic ring were

found at the end of the test. The solid-phase spectra of the TPEE/P–N showed that the interaction between the TPEE and P–N flame retardant improved the thermal stability and increased the residue at a high temperature of the composites for flame inhibition in the gas phase and the formation of the intermediate product through the interaction between aluminum ions with the carboxyl groups.

The decomposition of TPEE/P–N/Na-MMT in the solid residue at different temperatures is shown in Figure 8. The disappearance of typical bands (2956, 2861, and 1461 cm^{-1}) of the aliphatic groups at 400°C indicated that the addition of Na-MMT catalyzed the chain-scission reaction. The only typical bands at 1675 cm^{-1} were attributed to the electric charge of the metal ion to the carboxyl group. The metal cations (Si^{4+}/Al^{3+}) acted as Lewis acid sites and provided the basis for a coordinative interaction with the carbonyl group of TPEE. Apart from acting as a Lewis acid, the layered silicate facilitated the formation of double bonds that underwent crosslinking activity.[31] However, the result of the UL 94 test showed that the addition of Na-MMT failed in the UL 94 test in the presence of melt dripping. The addition of Na-MMT had a destabilization effect on TPEE/P–N for the catalytic action to the decomposition of TPEE.

Figure 9 gives the IR curves of TPEE/P–N/o-MMT during the heating process in an air atmosphere. There were three interesting regions in the spectra. One was located at 3600–3800 cm^{-1}. The peak at 3650 cm^{-1}, assigned to the P—O—H vibrations and indicating the partial intercalated structure of TPEE/P–N/o-MMT, decreased the release of diethylphosphinic acid during the heating process. Therefore, the barrier effect of o-MMT weakened the inhibition action in the gas phase and resulted in the decrease of the LOI value.

The second was the region at 2800–3100 cm^{-1}. The intensity of typical bands (2956, 2861, and 1461 cm^{-1}) of the aliphatic groups at 400°C, which indicated the partial intercalated structure of TPEE/P–N/o-MMT, also decreased the release of the pyrolysis products of TPEE. The peak at 3060 cm^{-1} was assigned to the —CH (aromatic ring) vibration. The layered silicate promoted the formation of double bonds that underwent crosslinking interactions and improved additional carbonaceous char at high temperatures.

The third region was also observed in the spectra of TPEE/P–N/Na-MMT at 1675 cm^{-1} and was attributed to the electric charge of the metal ion to the carboxyl group. The special structure of TPEE/P–N/o-MMT decreased the release of phosphoric acid and volatile products during the heating process; this promoted char formation and improved the char residue. A synergistic effect that increased the amount of residue was observed with the combination of the P–N flame retardant and o-MMT, and this corresponded to the results of TG. The practical intercalated structure enhanced the strength of the melt to prevent the dripping phenomenon during the combustion process. The synergistic effect in the condensed phase between the P–N flame retardant and o-MMT promoted dense and compacted char to prevent heat transfer and the release of volatile products. Therefore, TPEE/P–N/o-MMT showed the best thermal stability and fire resistance.
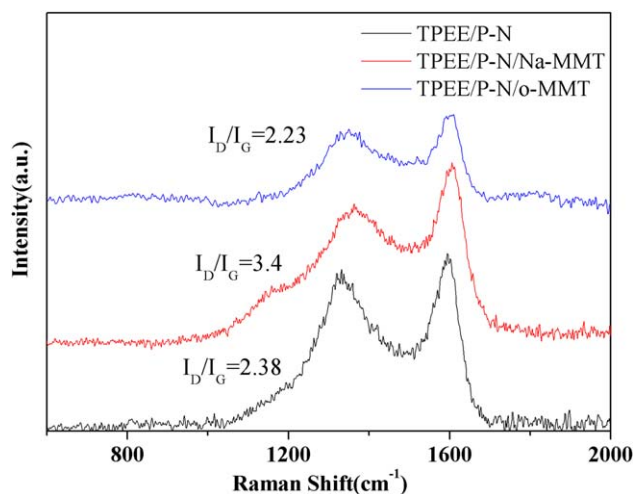
Figure 10. Raman curves of the char residues of TPEE/P–N, TPEE/P–N/Na-MMT, and TPEE/P–N/o-MMT after calcination at 800°C for 10 min in a muffle furnace. [Color figure can be viewed in the online issue, which is available at wileyonlinelibrary.com.]

Residue Analysis

Raman scattering is sensitive to the structural disorder of graphite. Laser Raman spectroscopy is a useful tool for characterizing the different types of carbonaceous structure formed during the combustion process. The residues of TPEE/P–N, TPEE/P–N/Na-MMT, and TPEE/P–N/o-MMT after calcination at 800°C for 10 min in the muffle furnace were used directly. From the Raman spectra of the residue, we found that a D band at 1352 cm^{-1} and a G band at 1600 cm^{-1} were present in the Raman spectra of all of the samples. The former band was attributed to the disordered graphite or glassy carbons, whereas the latter was ascribed to the stretching vibration mode with E_{2g} symmetry in the aromatic layers of the graphite crystalline. The degree of graphitization of the residual char was determined by the ratio of accumulated intensities of the D and G bands (I_D/I_G).[33] Basically, the lower the ratio of I_D/I_G was, the better the structure of the resulting char was. According to Figure 10, the incorporation of the Na-MMT into TPEE/P–N increased the I_D/I_G ratio tremendously compared to that of TPEE/P–N; this suggested a

decrease in the graphitization degree in the residual char. Furthermore, the incorporation of the o-MMT into the P–N flame retardants in TPEE decreased the I_D/I_G ratio in comparison with that of TPEE/P–N; this suggested an enhancement in the quality percentage graphitized carbons of the char. The graphitized char formed during the combustion process was significant in the control of the heat released and the release of volatiles for the stable char structure at high temperatures. The I_D/I_G ratio followed the order TPEE/P–N/Na-MMT (3.4) < TPEE/P–N (2.38) < TPEE/P–N/o-MMT (2.23) and showed that the highest graphitization degree and the most thermally stable char structure were found in formulation 4. The result of laser Raman spectroscopy confirmed that the graphitization degree of the residue was the highest of all of the samples; this resulted in the enhancement of the thermal stability and fire retardancy of the composites.

Figures 11–13 present SEM images of the residues acting as barriers. The study of the morphology and EDX analysis focused on the remaining residues of the TPEE/additives when neat TPEE was consumed and no residue remained at the high temperature. The residue morphology of formulation 2 is given in Figure 11. As shown in the image, there were a few obvious holes and flaws in the residue for the brittleness and strength of the char layer. Such a structure could not keep oxygen and heat away from the polymer matrix, so this resulted in only a V-2 classification for formulation 2 because of melt dripping.

Through the combination of P–N flame-retardant additives and Na-MMT, Figure 12 shows that different sized pores in the low-magnification image and well-dispersed uniformly sized holes in the char layer were formed at the high temperature. The catalytic effect of Na-MMT on the polymer chain, which resulted in the quick char-forming speed, which could slow down the escape of volatile decomposition products from the polymer and the counter diffusion of oxygen, reduced the polymer decomposition. However, the residue pore size varied; this was related to the dispersion of Na-MMT. In the presence of the pore, the materials still released the volatile gas to the air through the defected char and burned with flammable dripping so as to reach a V-2 ranking in the UL 94 test.
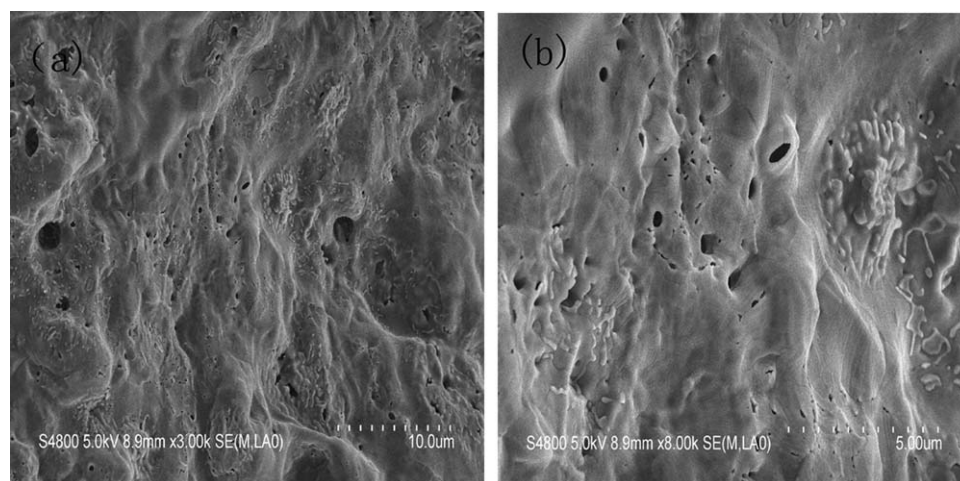

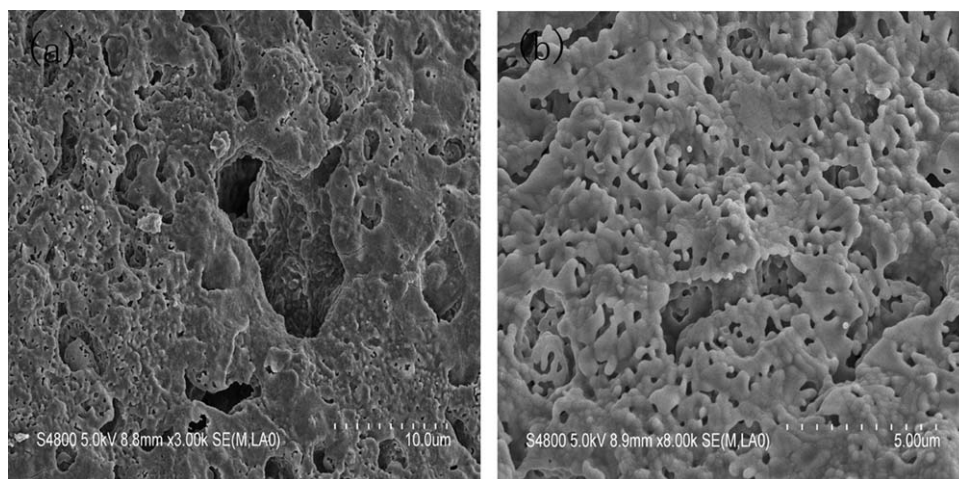**Figure 11.** SEM images of the residue for formulation 2 at (a) low (3000×) and (b) high (8000×) magnifications.

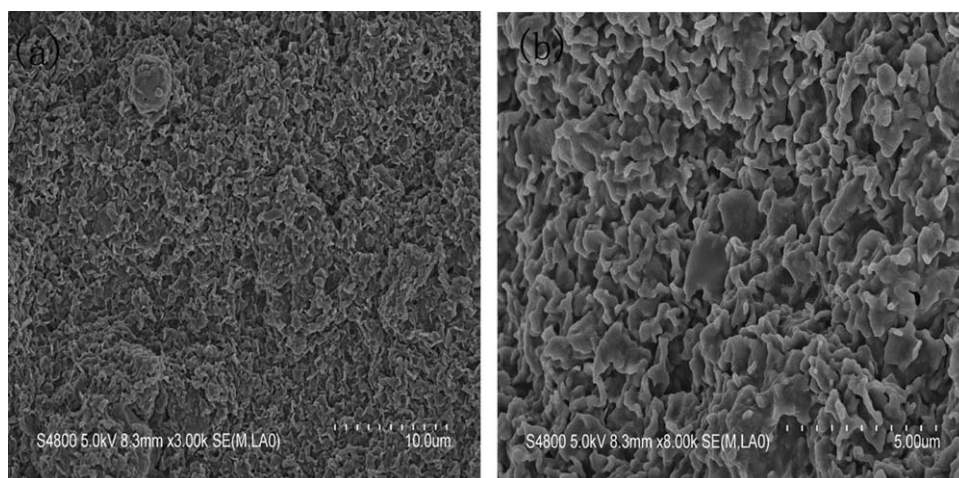**Figure 12.** SEM images of the residue for formulation 3 at (a) low (3000×) and (b) high (8000×) magnifications.

Figure 13. SEM images of the residue for formulation 4 at (a) low (3000×) and (b) high (8000×) magnifications.

Figure 13 shows the SEM image of the residual charred layer of TPEE/P–N/o-MMT. The addition of o-MMT obviously enhanced the quality of the char layer. The surface of the char layers became more integrated and compact. As highlighted in the figure, there was the presence of a folder structure morphology in the surface of the char layers for the deposition of carbonaceous residue on the surface; this was responsible for the enhanced thermal stability, improved flame retardancy, and higher char yield. The results indicate that o-MMT had a good synergistic char formation effect for the P–N flame retardant. The morphology of the char layer corresponded to the results of TG, FTIR spectroscopy, and laser Raman spectroscopy. For-

mulation 4 provided a V-0 classification because the compacted char effectively prevented the heat and mass from transferring to the air between the condensed phase and the gas phase.

The EDX elemental content of the residues is presented in Table VI. The residues consisted of carbon, oxygen, phosphorus, and aluminum. The content of oxygen corresponded to the thermal stability for the polymer combustion behavior, which was related to the polymer thermooxidative degradation. The residue had a lower content of oxygen; this resulted from inadequate combustion and indicated that the material had a better thermal stability.

Table VI. Elemental Contents of the Remaining Residue for the Flame-Retardant formulations

Material	C (wt %)	O (wt %)	Na (wt %)	Al (wt %)	Si (wt %)	P (wt %)
TPEE/P–N	7.79	61.17	—	13.18	—	17.86
TPEE/P–N/Na-MMT	7.26	61.53	0.74	12.56	3.33	14.57
TPEE/P–N/o-MMT	16.89	58.51	—	9.63	0.01	14.95

With the addition of o-MMT to the P–N flame-retardant TPEE composite, the carbon content in the residue increased obviously from 7.79 to 16.89 wt %. The content of carbon was ordered as follows: Formulation 2 ≈ Formulation 3 < Formulation 4. This was in agreement with the high weight residue of the TG test for the catalytic effect of layered silicates, which resulted in the quick decomposition rate of TPEE. The increase in the carbon content with the addition of o-MMT indicated that the intercalated layered silicate structure facilitated the crosslinking interaction and promoted the formation of additional carbonaceous char.

The content of oxygen was ordered as follows: Formulation 2 ≈ Formulation 3 > Formulation 4. The difference in the oxygen content also corresponded to the LOI value. Nitrogen was not found in the mapping area; this indicated that the nitrogen-containing content would have completely decomposed in the gas phase with the release of gas containing nitrogen, such as ammonia, at high temperatures.

In summary, o-MMT with the P–N flame retardant had a good flame-retardant synergistic effect on TPEE.

CONCLUSIONS

In this study, the fire properties of TPEE were investigated and compared with the flame-retarding TPEE. The combination of the P–N flame retardant with o-MMT helped to induce a significant fire-retardant effect in TPEE and render a V-0 classification in the UL 94 test. The TGA and DTG results indicate that the neat TPEE was consumed and no solid residue remained at 700°C. The weight of the solid residue increased several times more than that of neat TPEE because of the addition of the flame retardant and MMT. The combustion behavior testing showed that MMT catalyzed the decomposition of the polymer matrix and resulted in a decrease in the LOI value. The difference between Na-MMT and o-MMT containing materials resulted from the dispersion and microstructure of the PLSNs. The XRD and TEM results indicated the intercalated and partially exfoliated structure was formed in formulation 4 for the organic modification of MMT. The unique structure owned a barrier action, which could reduce the inhibition action of the P–N flame retardant and enhance the flame retardancy in the condensed phase. This implied more that phosphorus remained in the solid phase. The metal cations in the layered silicate could catalyze the chain-scission reaction. In addition, the metal cation promoted the formation of the aromatic product and resulted in an increasing amount of char residue at high temperatures. With the results of the Raman spectra and SEM–EDX, the synergistic effect between the P–N flame retardant and o-MMT on the condensed phase was proven. We confirmed that the catalytic effect on the crosslinking interaction was the main action of o-MMT.

REFERENCES

1. Lilaonitkul, A.; Cooper, S. *Rubber Chem. Technol.* **1977**, *50*, 1.

2. Sato, H.; Kondo, K.; Tsuge, S.; Ohtani, H.; Sato, N. *Polym. Degrad. Stab.* **1998**, *62*, 41.

3. Off. J. *Eur. Union* **2003**, *13*, L37.

4. Celebi, F.; Polat, O.; Aras, L.; Gündüz, G.; Akhmedov, I. M. *J. Appl. Polym. Sci.* **2004**, *91*, 1314.

5. Fischer, O.; Pospiech, D.; Korwitz, A.; Sahre, K.; Häußler, L.; Friedel, P.; et al. *Polym. Degrad. Stab.* **2011**, *96*, 2198.

6. Zhang, Y.; Chen, X.; Fang, Z. *J. Appl. Polym. Sci.* **2013**, *128*, 2424.

7. Wu, Q.; Qu, B.; Sun, M. *J. Appl. Polym. Sci.* **2009**, *114*, 562.

8. Gao, F.; Tong, L.; Fang, Z. *Polym. Degrad. Stab.* **2006**, *91*, 1295.

9. Fei, G.; Wang, Q.; Liu, Y. *Fire Mater.* **2010**, *34*, 407.

10. Wang, D.-Y.; Das, A.; Costa, F. R.; Leuteritz, A.; Wang, Y.-Z.; Wagenknecht, U.; et al. *Langmuir* **2010**, *26*, 14162.

11. Yang, F.; Nelson, G. L. *Polym. Degrad. Stab.* **2011**, *96*, 270.

12. Shen, Z.-Q.; Chen, L.; Lin, L.; Deng, C.-L, Zhao, J.; Wang, Y.-Z. *Ind. Eng. Chem. Res.* **2013**, *52*, 8454.

13. Sinha Ray, S.; Okamoto, M. *Prog. Polym. Sci.* **2003**, *28*, 1539.

14. Giannelis, E. P. *Adv. Mater.* **1996**, *8*, 29.

15. Gilman, J. W. *Appl. Clay Sci.* **1999**, *15*, 31.

16. Hu, Y.; Wang, S.; Ling, Z.; Zhuang, Y.; Chen, Z.; Fan, W. *Macromol. Mater. Eng.* **2003**, *288*, 272.

17. Ma, Z. L.; Zhang, W. Y.; Liu, X. Y. *J. Appl. Polym. Sci.* **2006**, *101*, 739.

18. Qin, H.; Su, Q.; Zhang, S.; Zhao, B.; Yang, M. *Polymer* **2003**, *44*, 7533.

19. Hao, X.; Gai, G.; Liu, J.; Yang, Y.; Zhang, Y.; Nan, C.-W. *Mater. Chem. Phys.* **2006**, *96*, 34.

20. Qin, H.; Zhang, S.; Zhao, C.; Hu, G.; Yang, M. *Polymer* **2005**, *46*, 8386.

21. Tang, Y.; Hu, Y.; Wang, S.; Gui, Z.; Chen, Z.; Fan, W. *Polym. Int.* **2003**, *52*, 1396.

22. Lecouvet, B.; Sclavons, M.; Bailly, C.; Bourbigot, S. *Polym. Degrad. Stab.* **2013**, *98*, 2268.

23. Wang, S.; Hu, Y.; Zong, R.; Tang, Y.; Chen, Z.; Fan, W. *Appl. Clay Sci.* **2004**, *25*, 49.

24. Zanetti, M.; Bracco, P.; Costa, L. *Polym. Degrad. Stab.* **2004**, *85*, 657.

25. Zanetti, M.; Costa, L. *Polymer* **2004**, *45*, 4367.

26. Abe, H. *Macromol. Biosci.* **2006**, *6*, 469.

27. Laoutid, F.; Lorgouilloux, M.; Lesueur, D.; Bonnaud, L.; Dubois, P. *Polym. Degrad. Stab.* **2013**, *98*, 1617.

28. Li, Y.; Li, B.; Dai, J.; Jia, H.; Gao, S. *Polym. Degrad. Stab.* **2008**, *93*, 9.

29. Xie, R.; Qu, B. *Polym. Degrad. Stab.* **2001**, *71*, 395.

30. Braun, U.; Bahr, H.; Sturm, H.; Schartel, B. *Polym. Adv. Technol.* **2008**, *19*, 680.

31. Gallo, E.; Schartel, B.; Acierno, D.; Russo, P. *Eur. Polym. J.* **2011**, *47*, 1390.

32. Levchik, S.; Camino, G.; Costa, L.; Levchik, G. *Fire Mater.* **1995**, *19*, 1.

33. Zhou, K.; Jiang, S.; Bao, C.; Song, L.; Wang, B.; Tang, G.; et al. *RSC Adv.* **2012**, *2*, 11695.